Elsevier Editorial System(tm) for Materials and Design
Manuscript Draft

Manuscript Number: JMAD-D-14-00069R2

Title: High Temperature Laser Sintering: An investigation into mechanical properties and shrinkage characteristics of Poly (Ether) Ketone structures

Article Type: Original Article

Keywords: Poly Ether Ketone, laser sintering, high temperature, mechanical, shrinkage

Corresponding Author: Dr. Oana Ghita,

Corresponding Author's Institution: Univeristy of Exeter

First Author: Oana Ghita, PhD

Order of Authors: Oana Ghita, PhD; O. Ghita; E. James; R Davies; S. Beretta; B. Singh; S. Flint; K.E. Evans

Abstract: This paper presents an investigation into the properties of Poly Ether Ketone (PEK) components using the commercial high temperature laser sintering system, EOSINT P800. The shrinkage and the mechanical performance of components across the entire build chamber have been tested and a non-linear shrinkage profile has been obtained. The middle of the build chamber recorded the highest degree of shrinkage and the shrinkage in Z direction had the largest variation. The laser sintered components built in X and Y directions recorded a 10% lower tensile strength than the injection moulded samples of the same material where those built in the Z direction showed an approximately 50% decrease in strength in comparison with the injection moulded test specimens. The crystallinity between the surface and the middle of the sintered samples was different; varied with the position within the build chamber and coincided with noticeable sample colour changes.

Highlights

- First study into fabrication of laser sintered Poly (Ether) Ketone (PEK) using EOSINT P800
- First detailed shrinkage map of the high temperature laser sintering system (HT-LS)
- First study to report results of mechanical data of PEK samples built in Z directions
- The surface and core of the PEK samples had 6% difference in crystallinity
- Strong colour changes were noticed across samples.

High Temperature Laser Sintering: An investigation into mechanical properties and shrinkage characteristics of Poly Ether Ketone structures

O Ghita[1*], E James[2], R Davies[2], S Beretta[1], B Singh[1], S Flint[2] and K E Evans[1]

[1]*University of Exeter, College of Engineering, Mathematics and Physical Sciences, North Park Road, EX4 4QF, UK*

[2]*Centre for Additive Layer Manufacturing (CALM), University of Exeter, College of Engineering, Mathematics and Physical Sciences, North Park Road, EX4 4QF, UK*

Abstract

This paper presents an investigation into the properties of Poly Ether Ketone (PEK) components using the commercial high temperature laser sintering system, EOSINT P800. The shrinkage and the mechanical performance of components across the entire build chamber have been tested and a non-linear shrinkage profile has been obtained. The middle of the build chamber recorded the highest degree of shrinkage and the shrinkage in Z direction had the largest variation. The laser sintered components built in X and Y directions recorded a 10% lower tensile strength than the injection moulded samples of the same material where those built in the Z direction showed an approximately 50% decrease in strength in comparison with the injection moulded test specimens. The crystallinity between the skin and the core of the sintered samples was different; varied with the position within the build chamber and coincided with noticeable sample colour changes.

Keywords: Poly Ether Ketone, laser sintering, high temperature, mechanical, shrinkage

[*] Corresponding Author information: Tel: +44 (0)1392 263667

Fax: +44 (0)1392 263616

E-mail address: O.ghita@exeter.ac.uk

1. Introduction

The Additive Manufacturing (AM) field has grown rapidly since its inception over two decades ago. The technological advances made in this field are pushing its application from prototype building to production of real parts. AM processes are now increasingly used by manufacturers especially for custom and short-run part production [1]. AM technologies offer many significant advantages when compared to traditional manufacturing methods such as the ability to produce complex freeform shapes, individually customised parts and significant reductions in material waste. Many of the polymeric materials available today on the market have reached their peak when it comes to possible applications and improved performance. The low glass transition temperature and melting temperature of most thermoplastic is a major limiting factor, which cannot be overcome by the addition of various reinforcements such as glass bead particulates [2], multi wall carbon nanotubes (MWCNTs) [3], silicon carbide [4], or aluminium [5]. Several attempts to use new, high temperature and high performance polymers have been tried in the past, with some degree of success. Most studies have focused on the process and equipment rather than the material and parts properties. The importance of a stable preheating temperature of 343 – 357°C has been highlighted by some of these studies [6], [7] as the equipment employed originated from a standard, low temperature, polyamide system and could not provide or maintain the high temperatures required for good sintering of PEEK.

Pohle et al., [6] decided to laser sinter PEEK by modifying an EOSINT P380 and application of a subsystem ("heating dome") able to preheat well the newly applied PEEK powder layers. The study did not comment on the new laser sintering process or the mechanical performance of the parts, focusing entirely on the cell vitality and proliferation.

Schmidt et al., [7] concluded that although the process is controllable within a wide range of laser energy applied, the preheating temperature range is rather small and the system requires a good protection of the hardware and good stability of the preheating temperature.

Tan et al., [8], investigated the quality of the PEEK-hydroxyapatite (HA) structures, using two bed temperatures (110 and 140°C) and a wide range of laser powers (9 to 28W) in a commercial laser sintering system. The authors noticed that higher bed temperature improves the quality of the sintering process, although delamination seems to affect many of the samples. Higher laser powers increased the degree of melting but the samples built at top laser power (28W) appeared charred. In order to achieve good integrity of the part it was proposed that the composition of PEEK-HA should be kept at 40% HA and sintered at 140°C bed temperature and 16W laser power.

Only one previous study [10] carried out by our group, focused on the physico-chemical behaviour of the material in high temperature laser sintering using the EOSINT P800 system [11]. Virgin and used HP3 PEK powders were thoroughly investigated in relation with the high temperature laser sintering process, the mechanical performance of HT-LS PEK parts was analysed as well as the levels of HP3 PEK powder reuse.

The poly-aryl-ether-ketone (PAEK) polymer family possesses excellent material properties including high stiffness and tensile strength, low weight, chemical and flame resistance and bio-compatibility, therefore making this range of polymers and their composites ideal for automotive, aerospace and medical applications. Traditional materials such as titanium and ceramics are being replaced by implantable PEEK polymer in a wide variety of components spinal fusion, hip replacement, cranio-facial and dental implants [12]. Use of PEEK polymer for metal replacement parts in the automotive industry and space applications, is becoming increasingly popular [13]. The high temperature stability and high continuous service temperature makes PEEK and their composites attractive bearing materials for wear applications [14].

The high temperature polymers are traditionally processed using extruders, injection moulding and compression moulding machines that operate at a temperature range of 371-400°C [15]. Conventional manufacturing techniques are normally suitable and economical for mass production purposes where the component design is relatively simple and can be accommodated by the injection moulding or compression moulding tool complexity. However, additive manufacturing technologies provide a degree of design freedom with the possibility of significant component weight reduction that is a key requirement for almost any new automotive or aerospace component. AM also enables the manufacturing of individually customized parts such as medical implants that would be both prohibitively expensive and time consuming using standard techniques. The combination of material properties and design freedom given by laser sintering makes this study highly interesting and inciting as it opens opportunities for new lightweight structures with complex designs.

Currently, polymers that can be processed at lower temperatures (less than 200°C) such as polyamide are widely used for the laser sintering purposes. A great deal of research has been conducted to examine the effects of the processing parameters of laser sintering on the resulting part properties of the polyamide parts including investigations into mechanical anisotropy due to part orientation and positioning [16], [17], 18], inconsistencies in the part properties due to the uneven thermal distribution in the build chamber [19], [20], and non-uniform shrinkage characteristics [21], [22]. For example, Gibson and Shi, [16], clearly

showed through experimental data that material properties (such as glass transition temperature and melting temperatures of powders and powder blends) are key factors in defining fabrication parameters and influence strongly the mechanical properties of laser sintered components. In addition to the materials properties and processing parameters, Gibson and Shi concluded also that orientation and build height levels can influence the mechanical properties of parts.

The use of a thermal imaging system by Wegner and Witt, [19], provided valuable insights into the temperature distribution during parts manufacturing which should be further explored to understand the relationship between material properties, part properties and processing parameters. The measurement of the melt temperature with identification of a sharp border between the molten area and the surrounding, un-molten powder is an important detail when trying to understand the shrinkage, crystallinity and mechanical properties of the laser sintered parts.

Soe et al., 2013, [22], carried out a thorough investigation of the shrinkage profile of test specimens and parts build in an EOS P700 system in Z direction. Clear trends were noticed and discussed in relation with the build height, size of the parts and repeat builds.

As a result of continued process improvements, some of the resulting mechanical properties of the laser sintered polyamide parts such tensile strength and modulus of elasticity are now comparable to injection moulded parts [23]. Some of these learnings will be transferable to the high temperature laser sintering systems.

The EOSINT P800 high temperature laser sintering system is capable of processing up to a temperature of 385 °C using EOS HP3 PEK (polyether ketone) material. Although the system has been available for few years, very little research has been carried out to map the EOSINT P800 system, and understand the effects of the high temperature laser sintering process on the resulting part properties [10], [24]. The objective of this research work is to investigate the HT-LS process using HP3 PEK powder with an aim to highlight the mechanical properties and shrinkage characteristics of the sintered parts.

2. Manufacturing of samples

2.1 Material

The material used for investigation is virgin EOS HP3 PEK powder [25]. Particle size analysis of the HP3 PEK powder has been presented elsewhere [10]. The powder particle distribution was as expected for laser sintering powders varying between 1 and 125µm with

the highest frequency between 37.5 and 63µm. Previous thermal studies of HP3 PEK powder [10] identified two melting peaks at 323.6°C and 372.5°C and 41.6% crystallinity, based on differential scanning calorimetry (DSC) measurements.

2.2 Design of build configuration

The goal of the test build was to provide data on key mechanical properties and dimensional variation in X Y and Z direction. The geometries chosen to form the build configuration were the ISO standard test sample geometries [26] for tensile testing. The bed had a maximum build volume of 700 mm × 380 mm × 580 mm.

Insert Figure 1

Figure 1 shows the distribution of the samples within the build chamber. A total of 162 specimens were built and tested. The samples were evenly distributed though out the three dimensional build area. This was motivated by the desire to evaluate variations of across the entire build chamber. In order to investigate further the shrinkage profile across the depth of the bed, samples in X direction were built at four depth levels: Z = 22, 54, 84 and 116 mm and in Y direction at two depth levels: Z=11 and 42 mm. In both cases, Z=0 mm represents the bottom of the build chamber.

Each sample was labelled with a unique code to identify it after removal from the powder bed once complete. This process is preferable to labelling the samples after part removal and reduces the risk of error.

The rear, right quarter of the available 3 dimensional build envelope was not used for building specimens as it is expected that there is symmetry within the build chamber in terms of thermal gradients and behaviour and therefore the samples built within the three quarters of the build chamber will suffice to provide a clear overview of the full build chamber profile.

The configuration of the build set-up was created using Materialise Magics RP v16 software. This is one of the most widely used software packages used in the additive manufacturing industry to manipulate STL files into grouped build configurations. The EOSINT P800 uses .SLI files to created 3 dimensional components directly from CAD data. The group of .STL files was sliced into 120µm layers using the standard EOS method and software [25].

2.3 EOS scaling components used for calculating shrinkage in the XY direction

The common method for addressing shrinkage in Laser Sintering is to apply a percentage increase in the X, Y and Z dimensions of the STL models prior to laser sintering. The method of calculating the correct values for xyz shrinkage compensation requires the laser sintering of test samples with no shrinkage compensation which are then analysed for dimensional accuracy against the original CAD model dimensions.

This method is commonly used by service engineers during system commissioning, and components manufactured by laser sintering are routinely measured against the original CAD data to monitor consistency and quality. This method can be used either by manually applying scaling factors to the component STL files during the job preparation, or by using a material dependent scaling factor set in the control software of the EOS laser sintering system, PSW3.5

The shrinkage compensation value calculated using the method described above was applied in MagicsRP to enable specific part placement and part collision avoidance. When applying a scaling factor to an STL model using MagicsRP, the change is applied from the geometric centre of the CAD model. When a scaling factor is applied as a material specific value in the EOS PSW control software, the change is applied from the software defined origin. Using PSW applied shrinkage compensation can lead to geometries overlapping in the build configuration, unless each layer of the build process is visually checked in the PSW software. This can ultimately result in co-joined components. For the purpose of this test procedure, applying the shrinkage compensation in MagicsRP allowed for the automatic collision detection function to be employed. The positional information of each component can also be exported from MagicsRP to allow accurate analysis of a large number of samples. The pre-applied scaling increase was set up at 4.95% in X direction, 5.07% in the Y direction and 4.5% in the Z direction.

2.4 Temperature calibration

The EOS P800 process chamber temperature is controlled through four infrared heating elements mounted at the upper front, back, left and right areas respectively. Temperature feedback is provided by a pyrometer that reads the powder surface temperature in the process chamber.

The removable frame temperature and building platform temperature are controlled by heating elements built into the removable frame. These are controlled independently of the

process chamber and are typically set at a lower temperature than the processing temperature in the laser sintering process.

Calibration of the heating of the process chamber is required to ensure uniform heating across the whole powder bed. It is already established that the power of the lamps and their positioning has a direct effect on the temperature uniformity of the powder bed surface [22].

The current method of calibration requires manual observation of the surface during the laser sintering of test crosses distributed across the build chamber. Typically the process chamber temperature is set to 10 °C below the manufacturers guidelines at the start of the calibration process. Once the layer upon which the test geometries is reached, the build process is paused after each layer. The freshly sintered cross sections show evidence of curling upwards when the powder bed temperature is too low. By incremental increases in the process temperature in between layers, the lower process temperature can be established. Observation of the test crosses also identifies colder zones in the process chamber, which can be compensated for by changes to the infrared heater configuration.

Once the lower processing temperature for successful laser sintering has been established, the temperature is further increased incrementally until visible discolouration of the powder bed is noted. This indicates that the upper processing temperature has been reached. The process temperature is then incrementally decreased until 9 °C below this point [22, 25]. An additional calibration procedure employed by EOS involves the use of an inline pyroscan device to scan the surface temperature of the powder bed. Variations in temperature are visible as different coloured regions in the pyroscan output images. Currently, the pyroscan hardware is not suitable for use with the elevated temperatures of the EOSINT P800.

The process chamber temperature was 365 °C, the build platform temperature was set up at 340°C and removable frame temperature was 345 °C.

2.5 Exposure settings and set up temperatures

The system manufacturer EOS has developed a new staged warm up phase of the automatic job start building process, to ensure a stable building process. The warm up cycle increases the temperatures in the process chamber and removable frame incrementally, allowing for temperatures to stabilise at each set point. During the automatic warm up phase, the recoating mechanism spreads several layers of new powder across the build chamber as the mechanism is moved from side to side. The operator can also specify a number of additional layers

before the building process commences. In this case, the removable frame upper position was set to 2.5 mm below the building plane and the automatic warm up process typically added 1.5 mm of powder.

The exposure strategy employed had a pre-contour of 8.5 W at 1000 mm x s^{-1} and an alternating hatch pattern of 15 W at 2550 mm x s^{-1} with a beam offset of 0.16 mm, and a hatching distance of 0.2 mm. The part exposure strategy across the build chamber was established by the PSW software replicating a non-structured part manufacturing setup, whereby the exposure order is not re-ordered after loading into the PSW software. The exposure strategies used were provided by EOS based on their internal optimisation process.

The post sintering was set to 12 seconds duration after exposure, as specified by EOS in the P800 operational manual [25]. The post sintering stage allows "the sintered powder grains to flow to form a homogeneous molten film" [25]. The energy applied during the standard sintering process may be insufficient to form a homogenous molten film with the material EOS PEEK HP3, hence the post sintering time at build temperature.

During the building process, the maximum layer time did not exceed the EOS recommended 90 second layer time [25]. The P800 standard cooling phase was used with 36h of nitrogen purge. The build chamber was allowed to cool down to room temperature before removal from the P800 and the build chamber transferred to the breakout station. The parts were manually removed from build chamber in a standard operating procedure and the samples stored at room temperature prior to testing.

3. Manufacturing of Injection moulding samples

The material used for injection moulding was VICTREX® HT G22, PEK injection moulding grade. HT G22, represents the PEK equivalent for injection moulding. PEK pellets were dried for 5 hours at 120 °C. Dog bone samples were manufactured as per manufacturer specifications. The nozzle temperature was 400 °C, injection hydraulic pressure was 900 bars for 2 seconds, the holding hydraulic pressure was 900 bars; injection speed was 60 cm^3 x s^{-1} and cooling time was 15 seconds.

4. Experimental Methods

4.1 Shrinkage measurements

All 162 samples were measured along their length with a Mitutoyo digimatic calliper in the X, Y or Z direction to find variation in shrinkage across the build bed. The tensile test specimens were built at 150 mm length. The shrinkage values were calculated using equation 1:

% shrinkage = ((Sample length – Model length) / Model length) x 100 (1)

The calculated values were used to create a robust shrinkage map across the build bed.

Injection moulded samples were not measured as the main interest in this study was to determine the shrinkage variation in the HT-LS process across the X, Y and Z directions.

4.2 Tensile testing

Tensile testing of the 162 sintered ISO 527-2-1A geometries [26] was carried out using a LLOYD instruments EZ20 mechanical testing machine at ambient temperature (20°C). Testing speed for all samples was 10 mm x min^{-1} breaking speed and gauge length 30 mm. 48 samples were tested for the X direction, 24 for Y direction and 90 samples in the Z direction. 20 injection moulded samples (40 x 5.5 x 2.0 mm) with a 25 mm gauge length were tested in a similar manner.

4.3. Colour observations

It was noticed that depending on the position of the samples in the build chamber the parts experience a significant change in colour. Optical images were taken using a Sony camera. Six samples were taken from Z direction located in the centre, X axis edge and Y axis edge of the build chamber as shown in figure 2. The two ends of the dog bone samples, with larger areas and often different surface colours had been used for analysis. All samples were polished on one side of the samples to expose the core area and to allow the analysis of the core of the sample. The surface of the selected samples was also analysed. Measurements from the surface of the specimens will be referred to as samples 1S to 6S; and measurements taken from the core of the sample will be referred to as samples 1C to 6C.

Insert Figure 2

4.4 X Ray Diffraction measurements

The samples selected in figure 2, had been further investigated using X-Ray diffraction. The technique measured the crystallinity changes incurred across the sample and identified any

correlation with the colour differences. X-ray diffraction analysis (XRD) was performed on the sintered parts directly using a Bruker D8 Advance X-Ray Diffractometer with a LynxEye detector, operating at 40kV voltage and 40mA current using CuKα radiation (λ=0.1542nm) in the 2θ= 5°-50° range in 0.05° increments.

4.5 Thermogravimetric Analysis (TGA)

The darker skin was separated ("shaved off") from the core of a sintered sample and its degradation behaviour has been investigated using a Mettler-Toledo TGA/DSC 1 system (LF1100 furnace type) equipped with a UMX5 balance. A blank calibration test was carried out prior to testing the sample. The samples were heated from 30 to 680 °C at 10 °C x min^{-1}. Following the same procedure as for the skin sample, core samples were also tested.

5. Results and discussion

5.1. Shrinkage measurements

Figure 3 shows sample average shrinkage for X, Y and Z directions across entire build chamber. It can be seen that the mean values for all three directions are lower than the model value of 150mm indicating that the correction shrinkage factor applied was underestimated. The largest variation in length was found in the Z samples. Figure 4 shows the Z shrinkage variation as a robust shrinkage map for samples across the entire bed.

For clarity, figure 4 presents the dimensional changes uncorrected (without application of the Z correction factor). Sample shrinkage can be seen to be largest in the centre and lowest around the outer walls of the build chamber, with a variation of 2.5% across the entire build chamber. Considering that the 4.5% is the pre-scaling factor applied for this build, the data plotted in figure 4 shows that the middle region of the build requires application of a higher pre-scaling factor, as currently, the parts are shrinking an extra 1.5%, where the edge samples are approximately 1% larger than they should be. Higher shrinkage means larger changes in the specific volume of the material as a function of processing temperature. In this case, the bed build temperature has a significant role in the shrinkage behaviour, the system building up higher thermal energy in the middle of the bed than on the edges. The region mapped in figure 4 represents approximately a quarter of the total build volume in Z direction. It is envisaged that the thermal variation will continue further within the depth of the bed, the thermal gradient possibly being the largest in the middle of the bed based on the additional X and Y maps produced at different Z depth.

Figure 5 and figure 6 show the shrinkage maps of the samples build in X and Y directions at different depth levels. Similar to figure 4, figure 5 and figure 6 presents the dimensional changes uncorrected (without application of the X and Y correction factors). The number of X and Y samples for each layer was relatively small in comparison with the samples built in the Z direction. Due to the process constrains (minimum space required between samples) and the design requirements for such a large build (presence of samples in all three directions uniformly distributed across entire bed chamber) it was not possible to accommodate larger number of samples at the selected depth levels.

In addition to the high thermal energy concentration noticed in the middle of the bed in relation to the X and Y coordinates, a higher shrinkage effect equivalent to a high thermal energy is noticed also across the depth of the bed at approximately 80-90mm from the bottom of the bed (see figure 5). As it can be also seen in figure 5, the bottom of the bed (Z = 22 mm) has the smallest shrinkage variation, where the top of build chamber (Z = 110-120 mm) retains some of the thermal energy accumulated from the top heaters during building and spreading of the last layers of powders.

Variation in part shrinkage across the build chamber in commercial laser sintering systems has been noted before by Shen et al., [27] and it was attributed to an uneven temperature distributions and cooling rates. Previous research on EOS P700 has found shrinkage values to vary by up to 2.5% with nylon 12 material depending on the depth of the build and the builds repeatability [20].

Insert Figures 3-6

5.2. Tensile testing

Figure 7 and 8 shows the variation in ultimate tensile strength and elongation to break of the samples for X, Y and Z directions. The Z direction samples show up to a 45% decrease in tensile strength and a 55% decrease in elongation to break when compared to the X and Y directions. The X and Y samples fractured at a tensile strength 10% lower than expected values. This anisotropy is commonly seen in ALM parts [28], although at a smaller extent, in general a decrease of up 20% in Z direction has been previously reported in nylon materials [17].

Insert Figure 7 & Figure 8

All samples tested failed in a brittle manner with the X and Y samples showing crack propagation from the skin of the sample and Z samples fracturing across the layer boundary.

As it can be seen in figure 8, the elongation at break is significantly lower in the case of laser sintered samples in comparison with the injection moulded values. This is a known feature of standard laser sintering manufacturing process, which shows a similar trend in high temperature laser sintering.

In this study, the experiments were carried out using standard processing parameters as proposed by the machine manufacturer. However, further optimisation is clearly required to allow good layer to layer bonding. It has been shown previously [18] that the energy density can influence the mechanical performance of the sintered parts, higher energy density leading to higher mechanical performance except for the highest energy density level which possibly leads to material degradation and therefore drop in mechanical performance.

5.3 Colour observations

Figure 9a shows the surface of the selected samples. An image of the cross section of a dog bone was also taken (see figure 9c) and a dark contour was noticed at the exterior of the sample, almost like a "crust" on the surface of the sample.

Insert Figure 9

5.4 X- Ray Diffraction (XRD) measurements

Table 1 presents the crystallinity results obtained from the XRD measurements from the surface and core of the selected sample specimens.

Insert Table 1

Table 1 shows that independent of the position of the sample within the chamber the crystallinity values within the middle of the samples are similar where the values measured at the surface of the samples are affected by their location within the build chamber. The samples with darker surface colour had an approximately 6% drop in crystallinity in comparison with the values measured in the middle which had always a lighter colour.

5.5 TGA measurements

It was suspected that the darker surface is the result of a thermo-oxidative degradation process which takes place during the manufacturing process. Day et al. [29], noticed similar colour changes when heating PEEK at 400°C for 6h in air and nitrogen, significantly more pronounced in air. The conditions used here are not entirely dissimilar to the ones used by Day et al. As stated in section 2.4, the system operates at 365°C chamber build temperature and the powder bed is slowly cooling over a period of 36h. In their study, Day et al., concluded that the discoloration is a combination of cross-linked network formation and increased conjugation in the remaining linear chain molecules. The thermogravimetric results shown in Figure 10 revealed also that the onset of degradation of the skin samples was approximately 15°C lower than the one of the cores, a clear indication of degradation. Similar to other studies [30], the TGA results obtained here showed significant mass loss happening below 600°C. Previous studies revealed a two stage degradation process with a lower mass loss in the second stage at temperatures above 600°C up to 1000°C.

Insert Figure 10

The correlation of figure 9 with table 1 shows that samples positioned at the bottom of the build presented the highest colour and crystallinity variation between core and skin, and therefore leads to the preliminary conclusion that cooling phase leads to the skin colour change. A longer residence time of the sample within the build chamber at higher temperature leads to a darker colour. Considering that the entire manufacturing process takes place in a nitrogen atmosphere similar to the nylon laser sintering systems, the strong change in colour was not expected. However, the high operating temperature of the system limits the functionality of the oxygen sensor in EOSINT P800, which is relatively far from the powder delivery point.

Although a large number of samples had been tested, it was not possible to determine whether the "crust" formed at the surface of some of the samples influences the mechanical properties of the test specimens as the colour variation was sometimes spread across the length of a sample as noticed in some of the samples selected for crystallinity measurements. Fully dark or light samples had been identified but the number of samples was not large enough to allow comparison.

6. Conclusions

This study represents the first investigation into the mechanical performance and shrinkage behaviour of HP3 PEK samples manufactured in the commercial high temperature laser sintering system EOSINT P800. The trends observed previously in laser sintering of nylon are present in high temperature laser sintering of HP3 PEK, although the effects are higher in the HT-LS: (1) mechanical strength in Z direction is lower than the value recorded in X and Y directions. The tensile strength reached an approximately 45% drop in tensile strength and 55% in elongation at break both in Z direction in comparison with X and Y directions, significantly lower values than those noticed in polyamides in the same direction; (2) the parts built are shrinking non-uniformly depending on thermal gradients and profile across the bed; (3) the residence time of the parts in the bed chamber at high temperatures affects the physico-chemical characteristics of the powder material and components built, having a much stronger effect on the part appearance than previously noticed in nylon. The exact implication the colour observations have on the parts performance is inconclusive at this stage. Controlled ageing testing of HP3 PEK powder and laser sintered parts could lead to a further understanding of the thermo-oxidative process and its relationship with mechanical performance.

The results demonstrated excellent prospective for high temperature laser sintering. Within the emerging area of additive manufacturing technologies and materials, standard/polyamides laser sintering reached maturity in comparison with HT-LS. The results presented here are the first to show performance of laser sintered PEK components. Further material development, hardware improvements as well as the knowledge gained in the development of polyamides laser sintering are expected to bring the quality of the components very close to well established manufacturing processes such as injection moulding.

References:

[1] Wohlers, T. Additive Manufacturing State of the Industry. Annual Worldwide Progress Report, 2010, Wohlers Associates Inc., Fort Collins,Co.

[2] Chung H, Das S. Processing and properties of glass bead particulate-filled functionally graded Nylon-11 composites produced by selective laser sintering, 2006, Mater Sci Eng A Struct Mater Prop Microstruct Process, vol.437:226, pp. 34

[3] Paggi R. A., Beal V.E., Salmoria G.V., Process optimisation for PA12/MWCNT nanocomposite manufacturing by selective laser sintering, 2013, Int J Adv Manuf Technol, Vol. 66, pp. 1977-1985;

[4] Gill T.J., Hon K.K.B., Experimental investigations into the selective laser sintering of silicon carbide polyamide composites, 2004, Proceedings of the Institution of Mechanical Engineers, Part B: Journal of Engineering Manufacture, vol. 218, no 10, pp. 1249-1256

[5] Mazzoli A. , Moriconi G., Pauri M.G., Characterization of an aluminium-filled polyamide powder for applications in selective laser sintering, 2007, Materials and Design, no. 28, pp. 993–1000

[6] Pohle, D., Ponader, S., Rechtenwald, T., Schmidt, M., Schlegel, K.A., Münstedt, H., Neukam, F.W., Nkenke, E. & von Wilmowsky, C., Processing of three-dimensional laser sintered polyetheretherketone composites and testing of osteoblast proliferation in vitro, 2007, Macromolecular Symposia 253(1), pp. 65-70.

[7] Schmidt, M., Pohle, D, Rechtenwald, T, Selective laser sintering of PEEK, 2007, CIRP Annals-Manufacturing Technology, no. 56/1, pp. 205-08

[8] Tan, K.H., Chua, C.K., Leong, K.F., Cheah, C.M., Cheang, P., Abu Bakar, M.S. & Cha, S.W., Scaffold development using selective laser sintering of polyetheretherketone-hydroxyapatite biocomposite blends, 2003, Biomaterials, no. 24(18), pp. 3115-3123

[9] von Wilmowsky, C., Vairaktaris, E., Pohle, D., Rechtenwald, T., Lutz, R., Münstedt, H., Koller, G., Schmidt, M., Neukam, F.W., Schlegel K.A. & Nkenke, E. 2008, Effects of bioactive glass and beta-TCP containing three-dimensional laser sintered polyetheretherketone composites on osteoblasts in vitro. Journal of Biomedical Materials Research - Part A 87(4), pp. 896-902.

[10] Ghita O.R., James E., Trimble R., Evans K.E., Physico-chemical behaviour of Poly (Ether Ketone) (PEK) in High Temperature Laser Sintering (HT-LS), 2014, Journal of Materials Processing Technology, vol. 214, pp. 969-978

[11] EOS, 2013, http://www.fkm-sintertechnik.de/content/docs/peek_hp3_englisch.pdf

[12] Kurtz S.M., Devine J.M., PEEK biomaterials in trauma, orthopedic, and spinal implants, 2007, Biomaterials, vol. 28, pp. 4845−4869

[13]Engineering Materials Magazine, Thermoplastics to revolutionise the composite industry, http://www.materialsforengineering.co.uk/engineering-materials-features/thermoplastics-to-revolutionaise-the-composites-industry/52151, June 2013,

[14] Lu Z.P., Friedrich K.,On sliding friction and wear of PEEK and its composites, 1995, Wear, vol. 181-183, pp. 624-631

[15] Margolis, J.M., 1985, Engineering Thermoplastics: Properties and Applications (Plastic Engineering). CRC Press. ISBN 0824780515

[16] Gibson I., Shi D., Material properties and fabrication parameters in selective laser sintering process, 1997, Rapid Prototyping Journal, Vol. 3 pp.129 – 136

[17] Ajoky U., Saleh N., Hopkins N., Hague R.J.M. , Erasenthiran P., 2006, Investigating mechanical anisotropy and end-of-vector effect in laser-sintered nylon parts. Proceedings of the Institution of Mechanical Engineers, Part B : Journal of Engineering Manufacture, 220 (7), pp. 1077-1086

[18] Caulfield B., McHugh P.E., Lohfeld S.,2007, Dependence of mechanical properties of polyamide components on build parameters in the SLS process, Journal of Materials Processing Technology, Volume 182, Issues 1–3, pp. 477-488

[19] Wegner A, Witt G, Process monitoring in laser sintering using thermal imaging, 2011, Proceedings of the Twenty Forth Annual International Solid Freeform Fabrication Symposium – An Additive Manufacturing Conference, Austin, Texas, USA

[20] Tontowi A. E., Childs T.H.C., Density prediction of crystalline polymer sintered parts at various powder bed temperatures, 2001, Rapid Prototyping Journal, Vol. 7 (3), pp.180 – 18

[21] Senthilkumaran K., Pandey P.M., Rao P.V.M., Influence of building strategies on the accuracy of parts in selective laser sintering, 2009, Materials and Design, no. 30, pp. 2946–2954

[22] Soe S. P., Eyers D. R., Setchi R., Assessment of non-uniform shrinkage in the laser sintering of polymer materials, 2013, The International Journal of Advanced Manufacturing Technology, Vol. 68, Issue 1-4, pp 111-125

[23] Drummer D., Rietzel D., Kühnlein F., Development of a characterization approach for the sintering behavior of new thermoplastics for selective laser sintering, 2010, Physics Procedia, Vol. 5, Part B, pp. 533-542

[24] Beard, M. A., Ghita, O. R., Bradbury, J., Flint, S., and Evans, K. E. (2011) Material Characterisation of Additive Manufacturing Components Made From a Polyetherketone (PEK) High Temperature Thermoplastic Polymer, Proceedings Advanced Research in Virtual and Rapid Prototyping (VRAP) (Bartolo, P. J., Ed.), Portugal

[25]http://www.eos.info/systems_solutions/plastic/systems_equipment/eosint_p_800, 2010, EOSINT P800 Operation Manual

[26] BS EN ISO 527-2:1996, Plastics-Determination of tensile properties-Part 2: test conditions for moulding and extrusion plastics

[27] Shen J., Steinberger J., Gopfert J., Gerner J., Daiber F., Manetsberger S., Ferstel S., 2000, Inhomogeneous Shrinkage of polymer materials in selective laser sintering.,

Proceedings of the Solid Free Form Fabrications Symposium, University of Texas, Austin, USA, pp. 298-305

[28] Hague R., Mansour S., Saleh N., Material and design considerations for rapid manufacturing, 2004, International Journal of Production Research, 42 (22), pp. 4691-4708

[29] Day M., Sally D., Wiles D.M., Thermal Degradation of Poly (aryl- Ether-Ether – Ketone): Experimental Evaluation of Cross-linking Reactions, 1990, Journal of Applied Polymer Science, vol 40, pp. 1615-1625

[30] Patel P., Hull R.T., McCabe R.W., Flath D., Grasmeder J., Percy M., Mechanism of Thermal Decomposition of Poly (Ether Ether Ketone) (PEEK) From a Review of Decomposition Studies, 2010, Polymer Degradation and Stability **95,** 709-718

List of captions

Figure 1 Test samples distribution in the build chamber (a) Z specimens positions (b) 3D image (X, Y, Z directions)

Figure 2 Samples selected for XRD testing

Figure 3 Sample length variations in the X, Y and Z directions

Figure 4 Shrinkage map of the P800 build chamber (based on z direction built samples)

Figure 5 Shrinkage map of the P800 build chamber (based on x direction built samples)

Figure 6 Shrinkage map of the P800 build chamber (based on y direction built samples)

Figure 7 Tensile strength of HP3 PEK sample built in X, Y and Z direction and injection moulded samples.

Figure 8 Elongation at break of HP3 PEK sample built in X, Y and Z direction and injection moulded samples

Figure 9 (a) Optical images of the skin of the six samples (1S to 6S), (b) Optical images of the core of the six samples (1C to 6C); (c) Optical image of the cross section of a dog bone

Figure 10 Onset degradation temperature for skin and core samples

Table 1 XRD crystallinity measured values from surface and core samples

Skin measurements/ % Crystallinity	**Core measurements/ % Crystallinity**
1S/ 26.3	1C/ 34.4
2S/ 32.3	2C/ 33.1
3S/ 22.1	3C/ 34.8
4S/ 31.6	4C/ 34.2
5S/ 27.0	5C/ 35.8
6S/ 31.8	6C/ 34.3

Table1

Skin measurements/ % Crystallinity	Core measurements/ % Crystallinity
1S/ 26.3	1C/ 34.4
2S/ 32.3	2C/ 33.1
3S/ 22.1	3C/ 34.8
4S/ 31.6	4C/ 34.2
5S/ 27.0	5C/ 35.8
6S/ 31.8	6C/ 34.3

Figure1a

Click here to download high resolution image

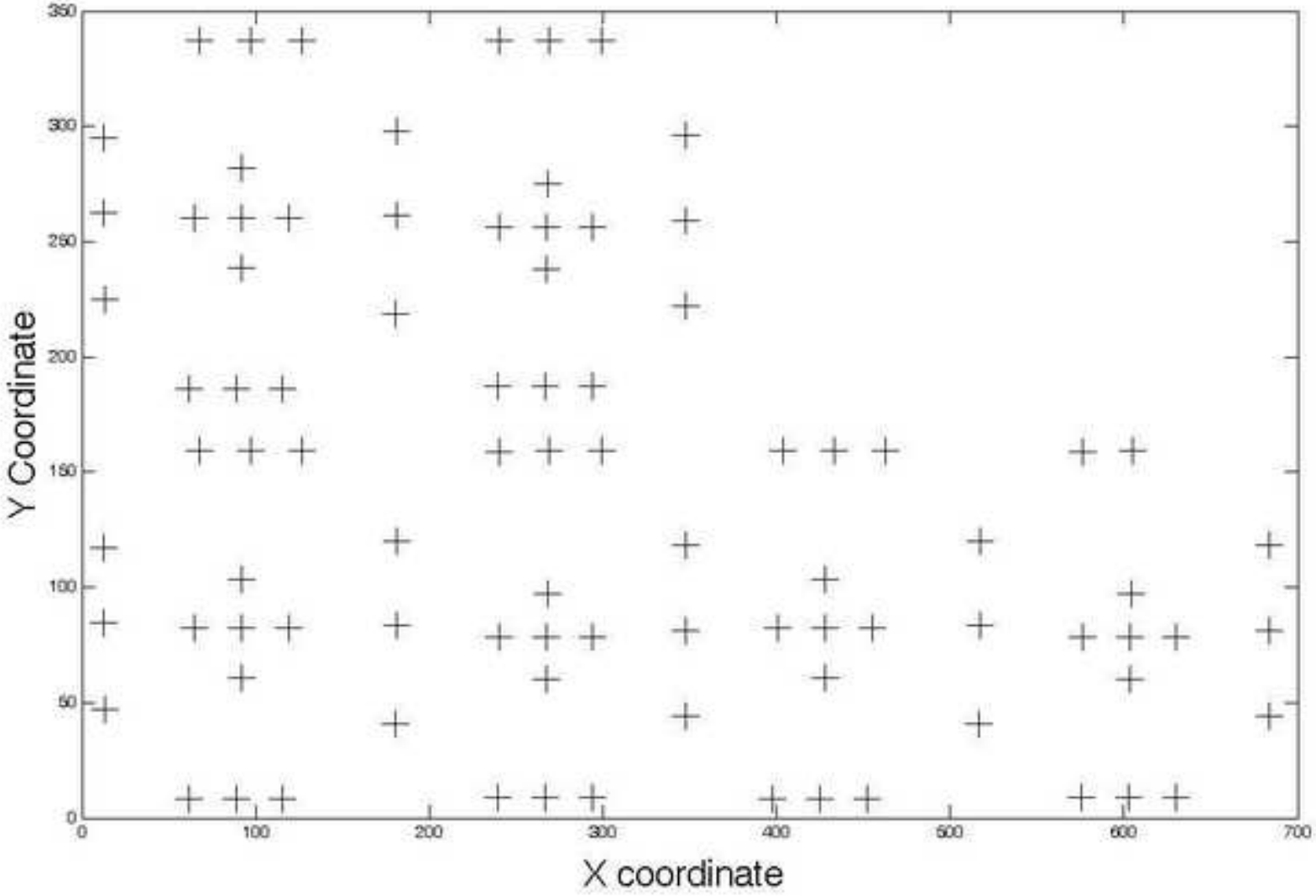

Figure1b

Click here to download high resolution image

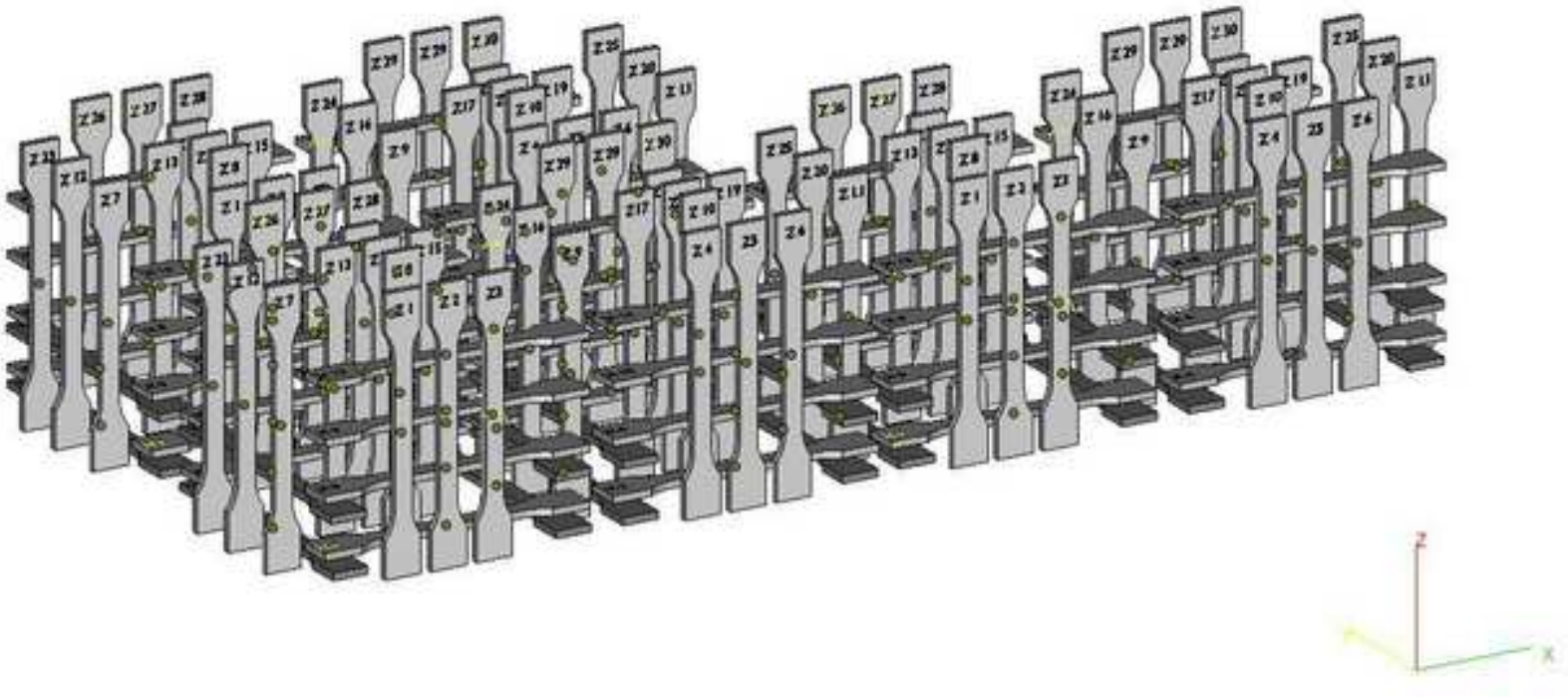

Figure2

Click here to download high resolution image

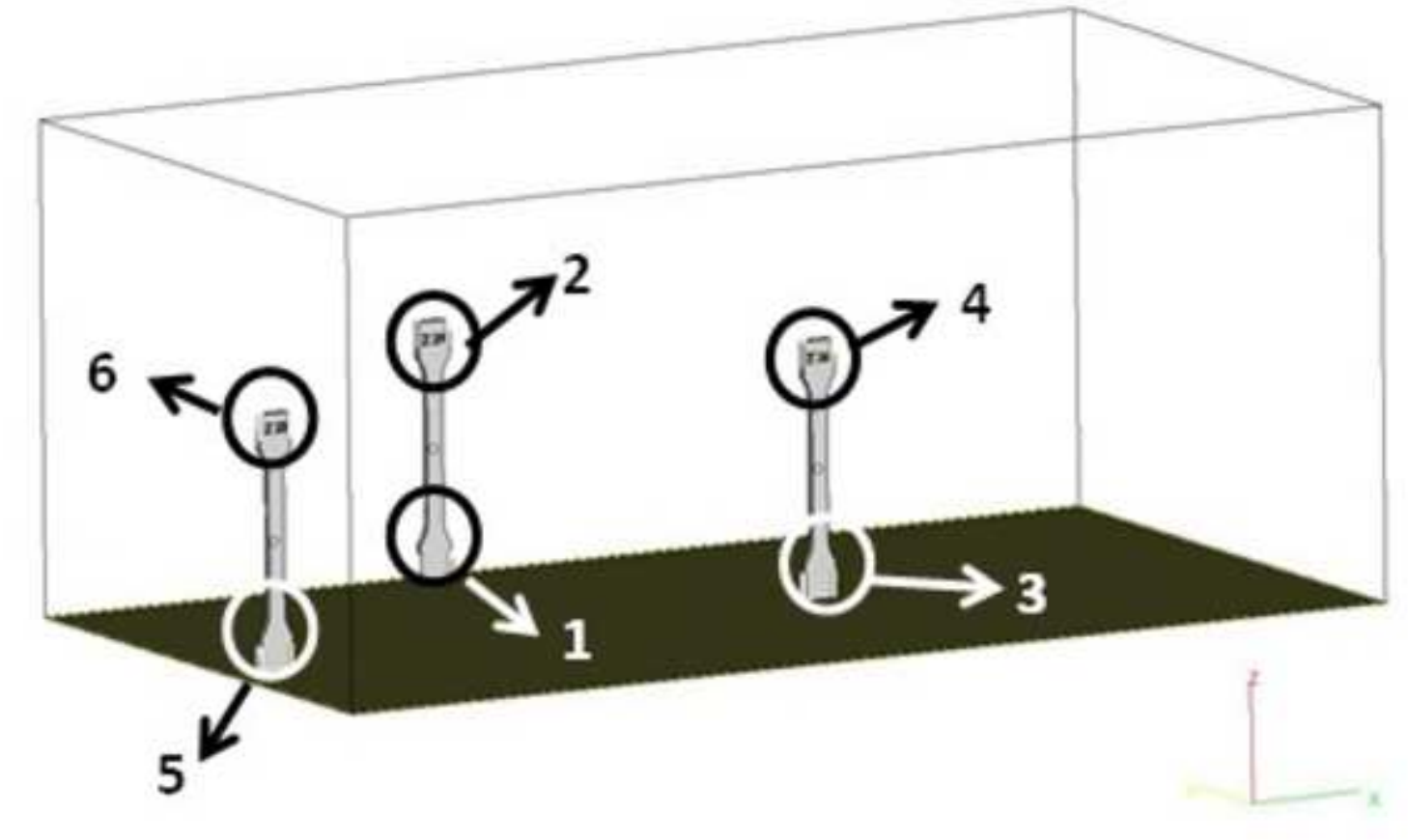

Figure3
Click here to download high resolution image

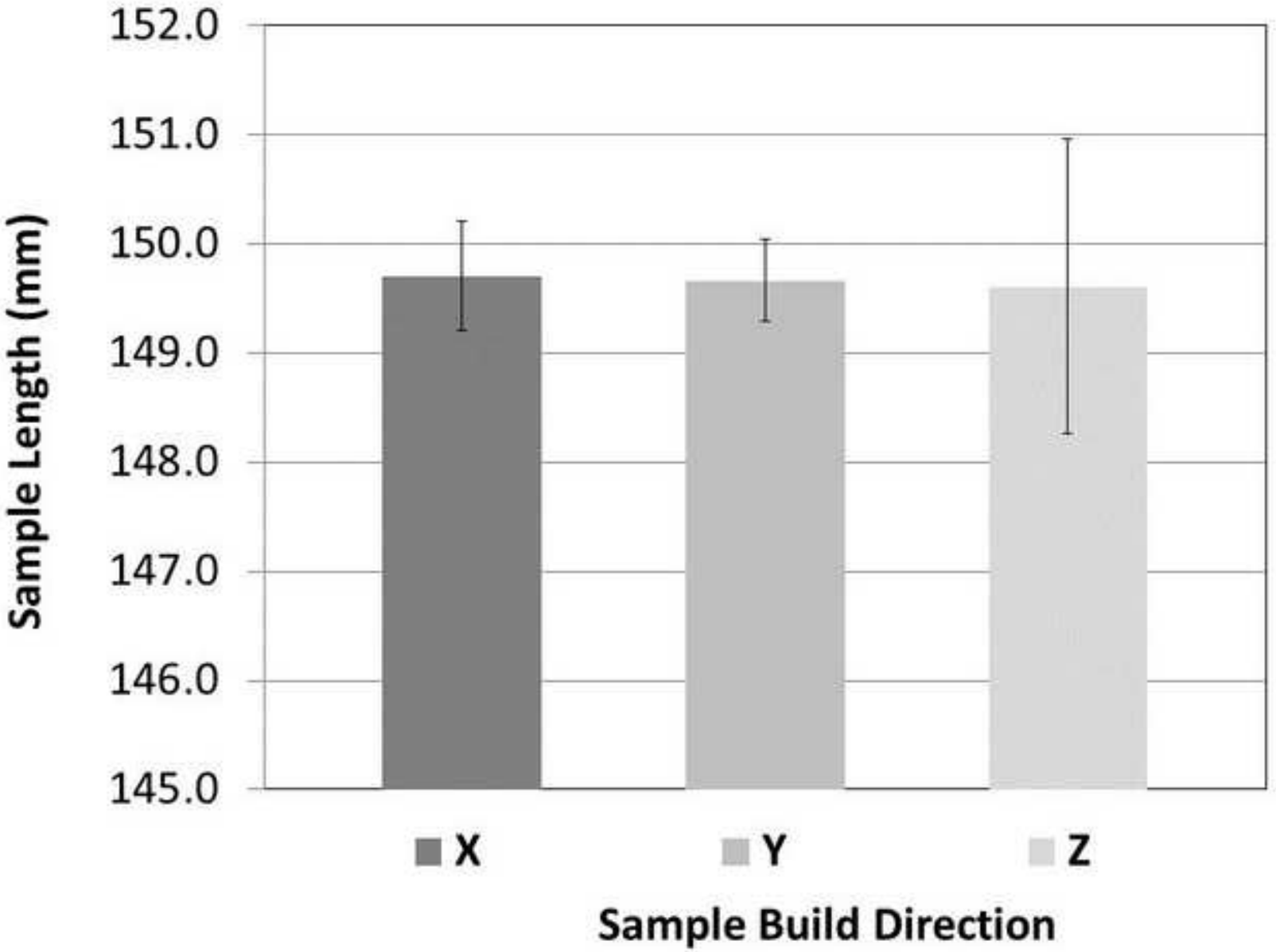

Figure4

Click here to download high resolution image

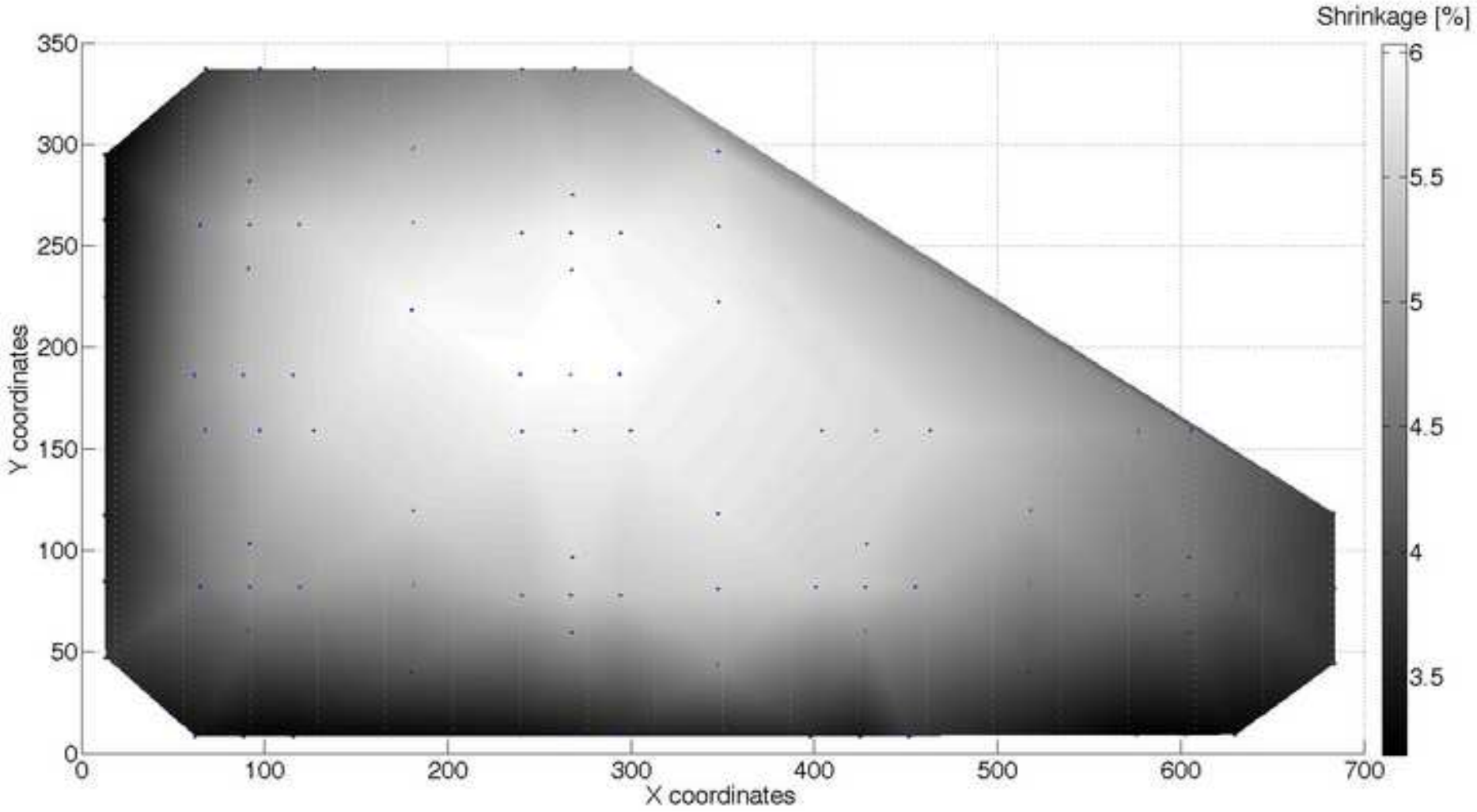

Figure5
Click here to download high resolution image

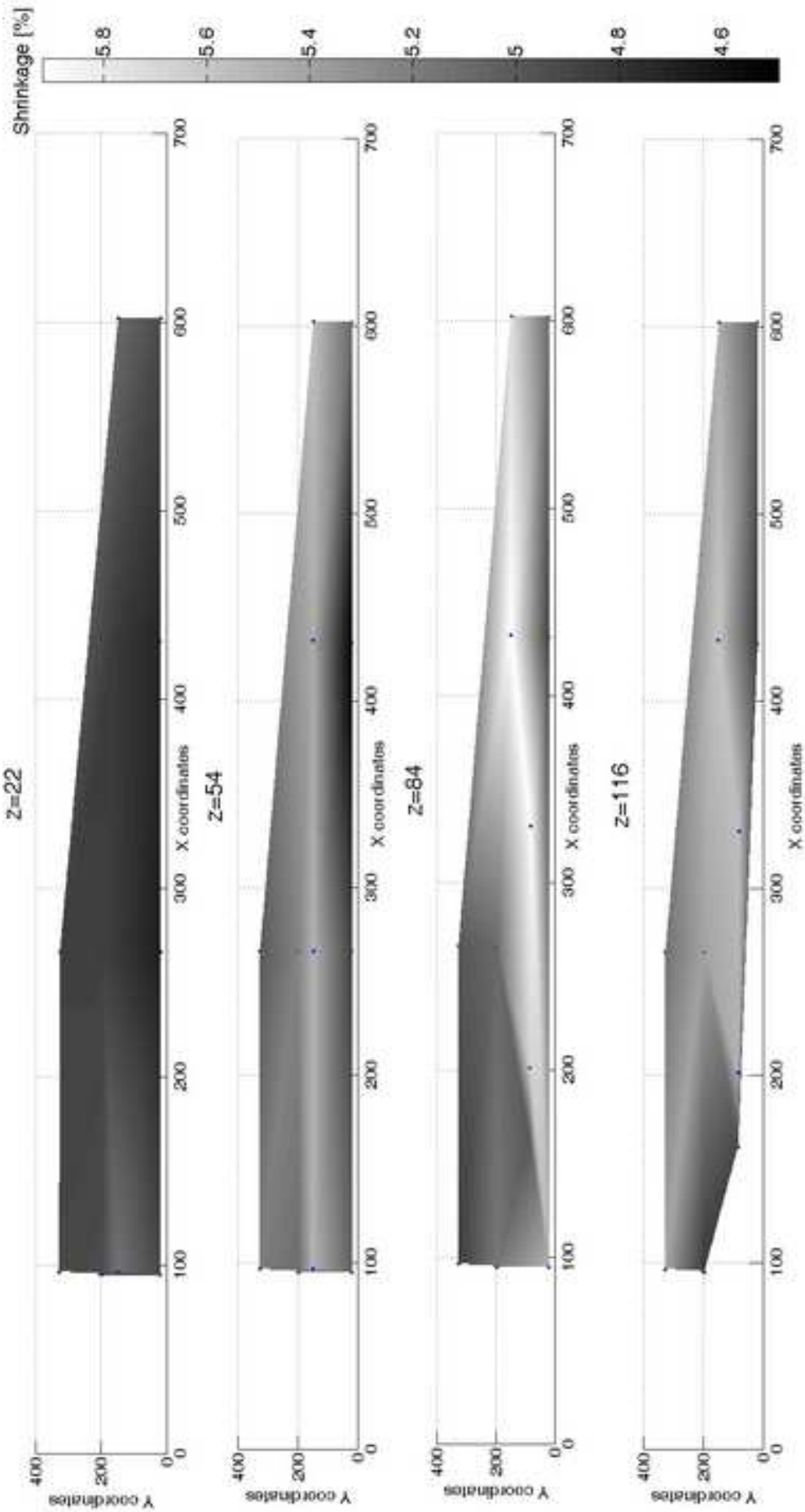

Figure6

Click here to download high resolution image

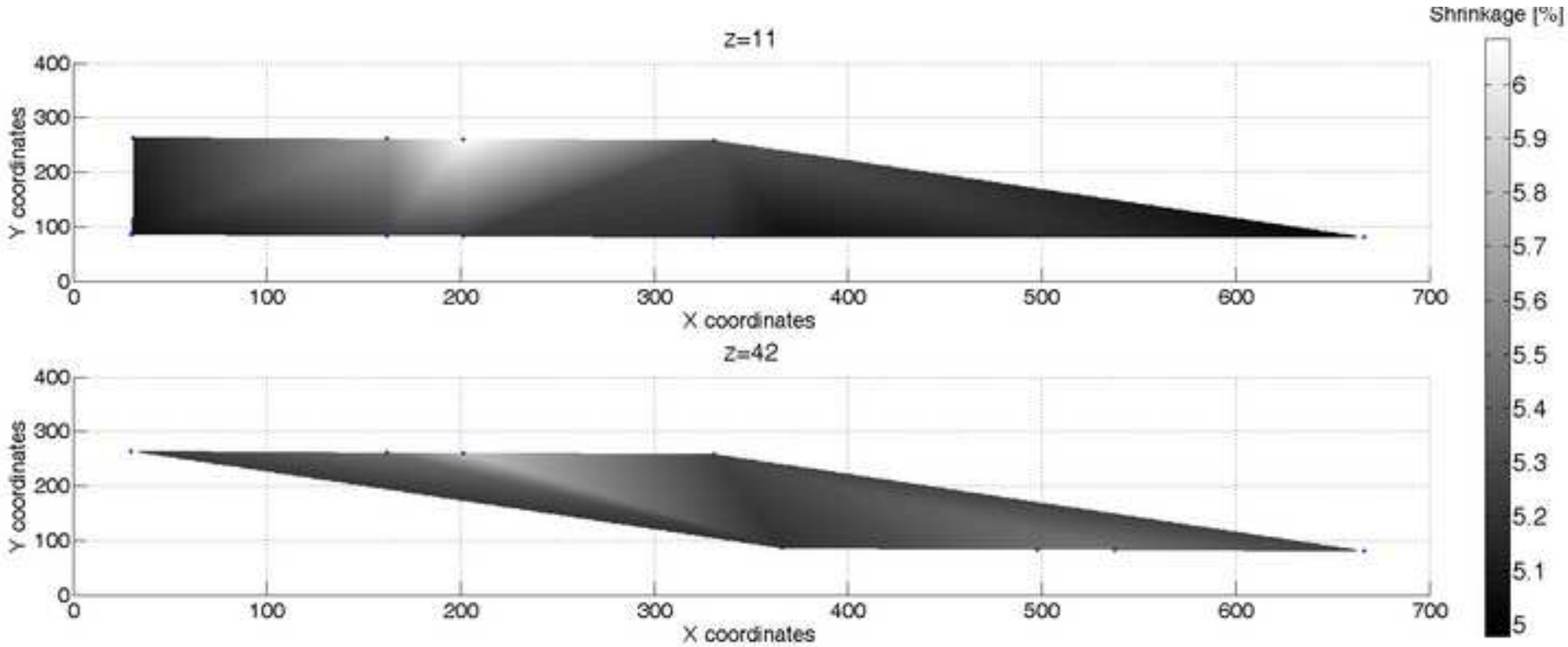

Figure7
Click here to download high resolution image

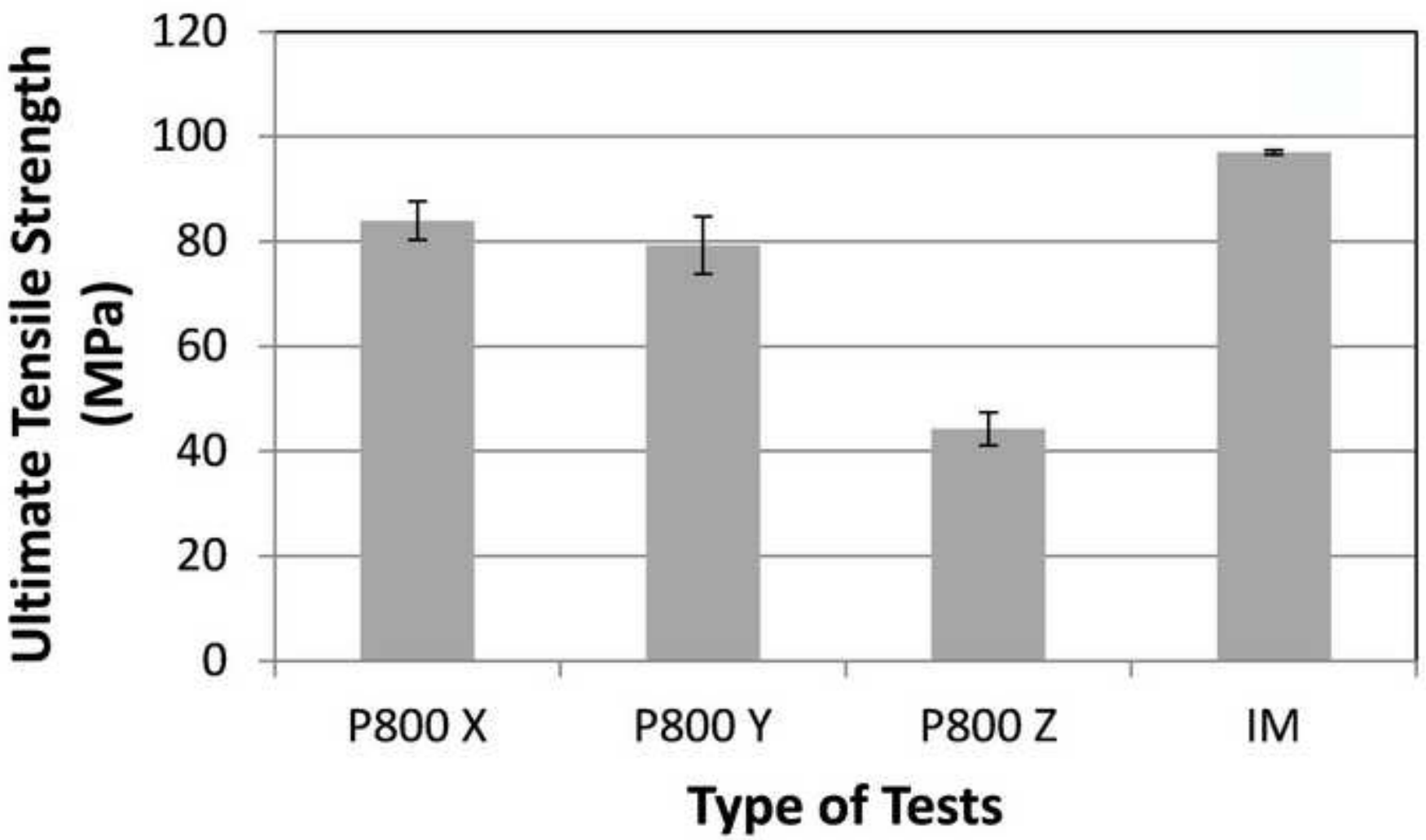

Figure8
Click here to download high resolution image

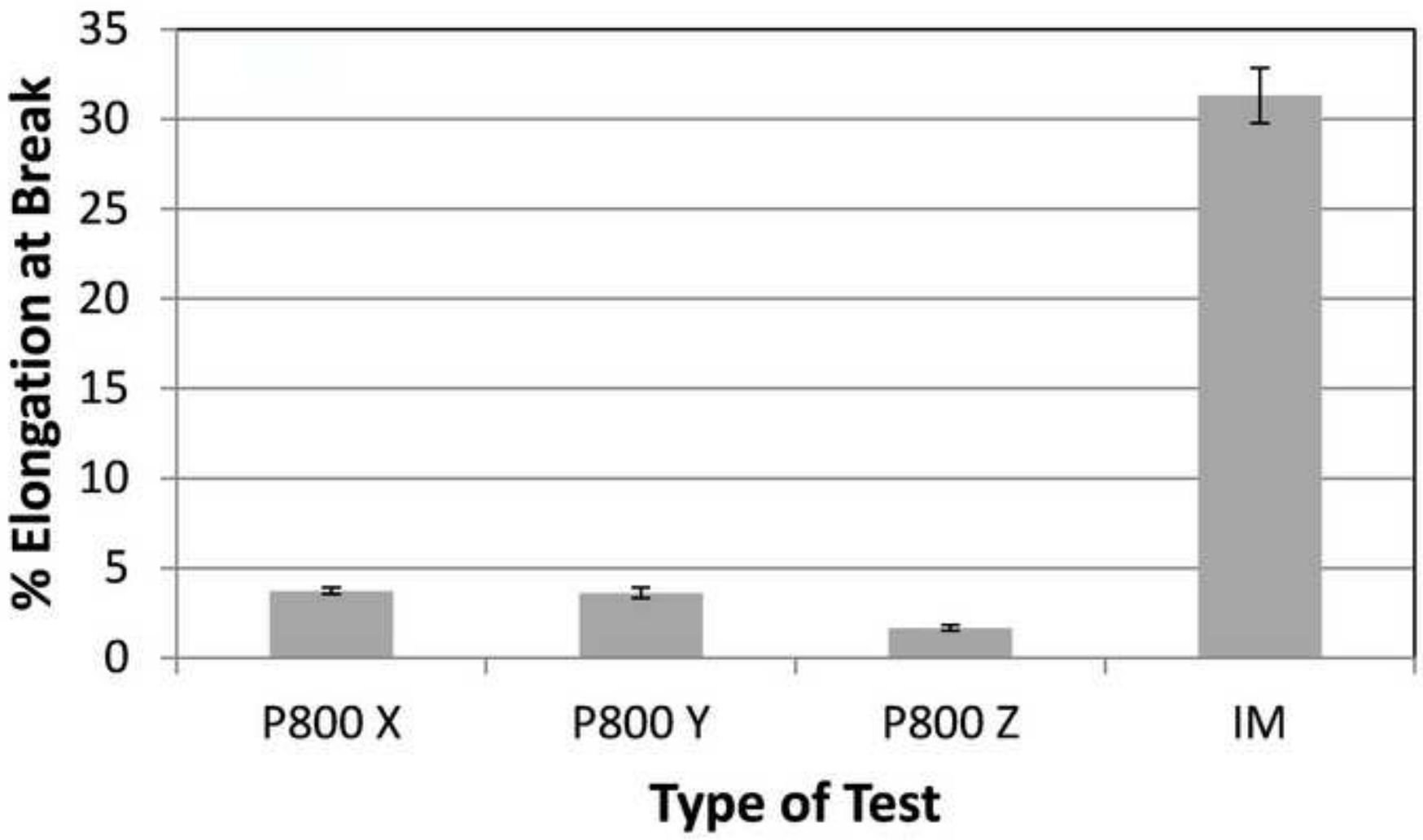

Figure9a
Click here to download high resolution image

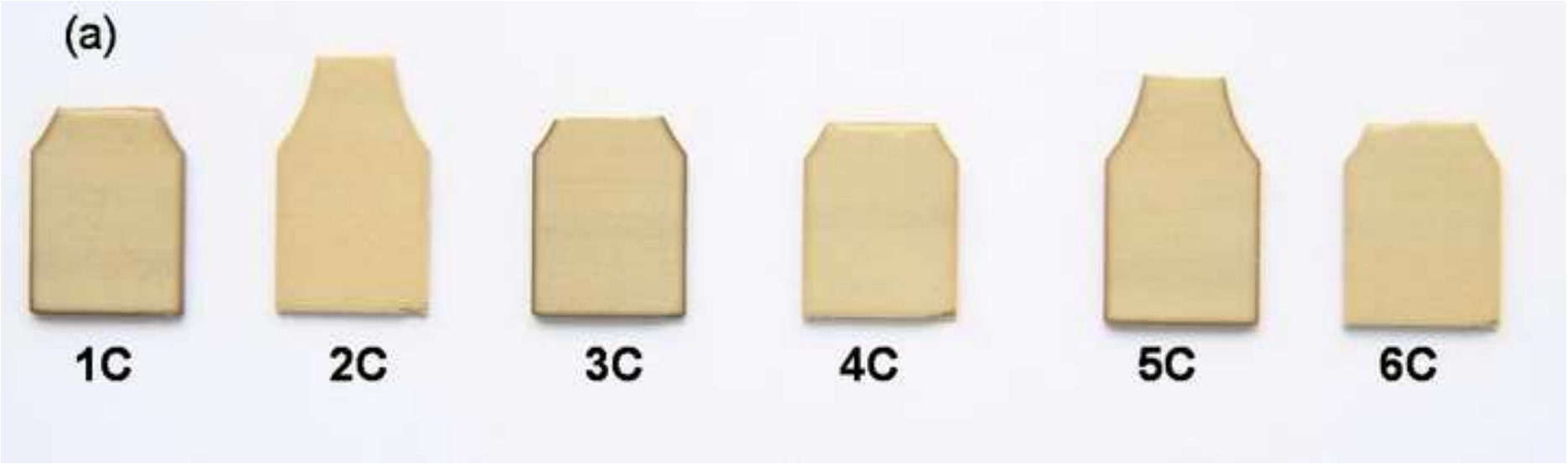

Figure9b

Click here to download high resolution image

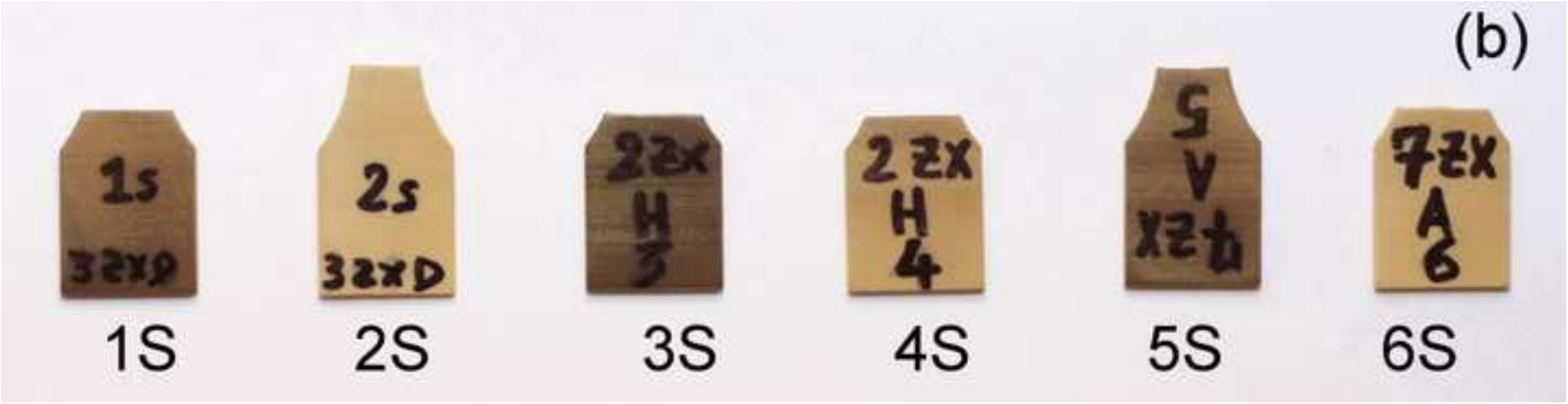

Figure9c
Click here to download high resolution image

Figure10
Click here to download high resolution image